This document is the accepted manuscript version of the following article:
Araujo, D. M., Auchmann, B., Brem, A., Daly, M., Hug, C., Michlmayr, T., … Milanese, A. (2024). Assessment of training performance, degradation and robustness of paraffin-wax impregnated Nb3Sn demonstrator under high magnetic field. IEEE Transactions on Applied Superconductivity. https://doi.org/10.1109/TASC.2024.3368995

Assessment of Training Performance, Degradation and Robustness of Paraffin-Wax Impregnated Nb_3Sn Demonstrator under High Magnetic Field

D. M. Araujo, B. Auchmann, A. Brem, M. Daly, C. Hug, T. Michlmayr, K. Amm, M. Anerella, A. Ben Yahia, J. Cozzolino, R. Gupta, P. Joshi, M. Kumar and A. Milanese.

***Abstract*—In the context of high-energy physics, the use of Nb_3Sn superconducting magnets as a cost-effective and reliable technology depends on improvements in the following areas: long development and manufacturing cycles, conductor degradation after thermal cycling, long training, as well as a demonstration in accelerator magnets with a beam aperture of the full potential of modern Nb_3Sn conductors. In short, performance, robustness, and cost are the three issues to be addressed. The Magnet Development project (MagDev) of the Swiss Accelerator Research and Technology initiative (CHART) at the Paul Scherrer Institute (PSI) aims to contribute to the solutions to each of these issues, re-thinking the manufacturing and design process. In our program, every innovation is to be validated by means of a panoply of fast-turnaround tools: from non-powered and powered samples and coils, tested under background field, to low-field subscale magnets and high field short prototypes. This work presents one element in this panoply of R&D vehicles: a stress-managed Nb_3Sn coil called BigBOX, impregnated with paraffin wax, and tested, through a collaboration with the Magnet Development Program of the United States (US-MDP), in the background field of Brookhaven National Laboratory (BNL)'s common coils dipole DCC17.**

***Index Terms*—Superconducting Magnets, High field magnets, Magnet R&D, Magnet technology.**

I. INTRODUCTION

Answering to the European Strategy for Particle Physics (ESPP) update [1], CHART pursues Nb_3Sn accelerator magnet R&D with the goal of improving the performance and robustness of state of the art high-field superconducting magnets based on Nb_3Sn Rutherford cables. In this contribution, we aim to produce a coil demonstrator that solves issues of conductor degradation by means of stress-management, and issues of long training in stress-managed magnets by means of wax impregnation.

To mitigate the risk of mechanical degradation during assembly, we rely on a concept where no pre-load or a very limited one is transferred to the coil, even if the magnet structure is pre-loaded. To manage the mechanical loads during the powering phase, stress-management structures are investigated, which are now the main focus of our R&D work, and have been studied at different labs for different magnet structures, like canted cosine-theta [2], block-type [3], [4] and cosine-theta [5].

If the stress-managed concepts without pre-load may help on the degradation issue, the question about training remains challenging. The training curve is strongly linked to crack-induced energy release in the coil's composite matrix, as well as debonding between the impregnated coil and the surrounding components. Recent BOX experiments showed fast training curves, or even absence of training, in single turn wax impregnated Nb_3Sn Rutherford cable in a stress-managed situation [6]. Moreover, wax-impregnated Rutherford cable was exposed to transverse stress, showing that the conductor support may be sufficient for a stress-managed coil that exhibits relatively low coil stress in operational conditions. At the same time, we note that the use of wax during the impregnation process makes room temperature pre-load on the coil impossible.

By combining all elements discussed before, our high-field magnet development program for now studies pre-load less, stress-managed magnets, impregnated with paraffin wax and enclosed into a confined structure. Other solutions, like filled-wax or filled-epoxy impregnation, are under study. Before building standalone magnets, we decided to probe whether the results from single-turn samples hold up in a block of turns under representative Lorentz forces. To achieve this, a racetrack-shaped demonstrator, called BigBOX, was manufactured and is to be tested under background field.

An overview of this paper is as follows: section II briefly describes the test facility in which the coil is going to be tested. Section III presents a 2D coil test design, strand and cable properties. Section IV discusses the integration of the coil test into DCC17 with 3D magnetic and mechanical models and analyses. In section V, some details on the coil manufacturing process and technology are presented. Section VI presents an extension of these studies due to the upgrade of the test facility, before the test could take place, which resulted in the possibility of increasing the coil current while operating DCC17 at lower field level. Finally, the results are presented and discussed in sections VII and VIII.

II. DCC17: BNL Nb_3Sn DIPOLE

DCC17 is a common-coil dipole, designed and manufactured at BNL, which is operated as a test bench for LTS and HTS conductors and samples. The magnet is based on React & Wind technology, it has a wide, but narrow free

aperture and a straight section of about 300 mm. Table 1 shows some of the DCC17 relevant parameters [7].

TABLE I
DCC17: BNL Nb_3Sn DIPOLE

Parameter	Value	Unit
Conductor type	Nb_3Sn	-
Magnet Technology	React&Wind	-
Free aperture	29 x 335	mm^2
Separation between magnetic centers	236	mm
Straight section length	304.8	mm
Temperature T_{op}	4.2	K
Short sample current I_{SS} at 4.2 K	10.8	kA
Short sample bore field B_0 at 4.2 K	10.2	T
Short sample coil peak field B_{SS} at 4.2 K	10.7	T
Self-inductance	4.9	mH
Stored Energy at I_{SS}	0.2	MJ
Conductor type	Nb_3Sn	-

The magnet (see Fig. 1 left and center) has two high-field volumes, which allow running two independent tests at once, or avoiding thermal cycles to change between two samples. Because of these characteristics, we decided to use only one side of the aperture, as shown in Fig. 2. Before getting to the 3D design and integration, in Section IV, we present the 2D design.

III. Nb_3Sn Coil

In this section, we consider the coil 2D cross-section. The goal is to accumulate mechanical stress, exclusively due to Lorentz forces since no-pre-load is applied, in one leg of the coil and on its flat surface. Fig. 1 right shows directions of field and current to obtain this goal.

The coil has been wound in the hard way direction and is composed of 13 turns. Coil parameters are presented in Table 2 and strand ones in Table 3. The cable's ID provided by LBNL is 942 and was manufactured in 2006 for the LARP program [8], [9].

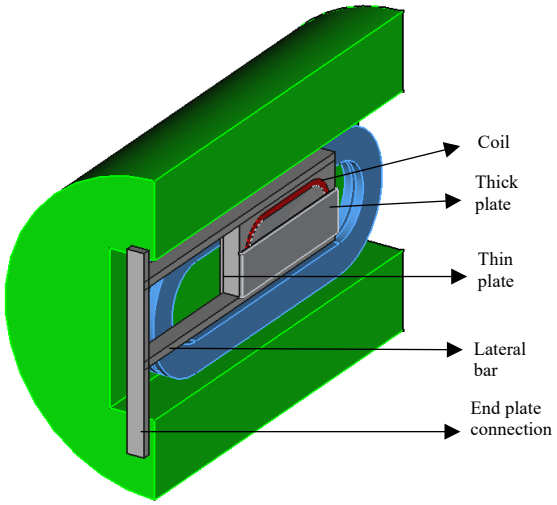

Fig. 2. 3D Mechanical integration. The coil is shown in yellow in between plates that help to reduce the induced stress onto the common coils.

TABLE II
MAJOR Nb_3Sn COIL PARAMETERS

Parameter	Value	Unit
Number of turns	13	-
Cable bare width	7.79	mm
Cable bare thickness	1.28	mm
Insulation thickness	155	µm
Number of strands	20	-
Nominal current (I_{op})	10	kA
Nominal background field (B_0)	10	T
Temperature T_{op}	4.2	K
Self-inductance	0.078	mH
Stored Energy at I_{op}	3.9	kJ
Straight section	100	mm
Inner radius	60	mm

To connect the Nb_3Sn coil leads to the test station bus bars, each lead has been spliced to Nb-Ti cables, also used in reference [10]. To carry the high current, and because of self

Fig. 1. Left: Superconducting common coils magnet DCC17 view from the end plate. Center: Structure for assembling samples into DCC17. Right: Coil electric current I_{bb}, Background field B_{cc} and coil magnetic force F direction.

and background field, two Nb-Ti cables are used for each Nb_3Sn lead.

TABLE III
RRP OST 54/61 STRAND PARAMETERS

Parameter	Value	Unit
Strand	RRP OST 54/61	-
Diameter	0.7	mm
Cu/no-Cu	0.87	-
I_C (12 T, 4.2 K)	551 - 572	A
Strand RRR before cabling	188 - 201	-

In order to map out the relevant operational conditions for stress-managed coils, we designed to test it at least up to the level of 160 MPa.

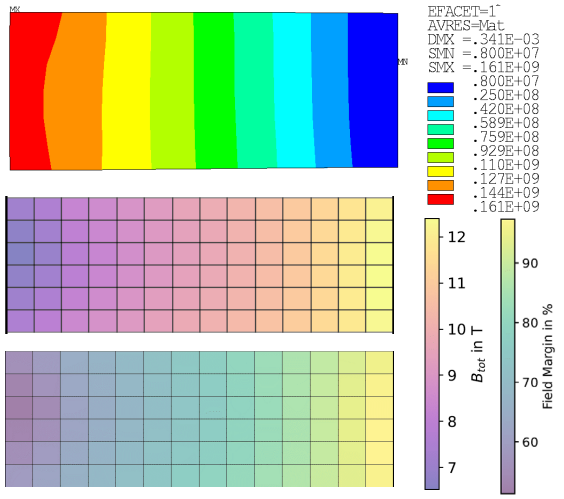

Fig. 3. Von-Mises stress in Pa, Magnetic field in T and Field Margin in percentage.

Fig. 3 shows Von-Mises stress, total magnetic field and field margin all along the 13 turns of the coil. Because of the nominal self-field contribution, of around ± 2.5 T, the high stress region sees a lower field than the background field and the low stress region sees a higher field. The calculation results presented in Fig. 3 were obtained with 2D models. The coil was modelled as homogenized isotropic material with a Young's modulus of 25 GPa. The configuration generates a wide range of stress/margin combinations that may allow to glean relevant insights into the mechanically-induced performance reduction or degradation. Further studies are presented in section VI.

IV. MAGNETIC AND MECHANICAL INTEGRATION INTO DCC17

This section describes the magnetic and mechanical integration of the Nb_3Sn coil into DCC17. Paragraph IV.A describes the magnetostatic model and results, while paragraph IV.B discusses some aspects of the mechanical model and results.

A. Magnetic Analysis

The models, produced in 3D Maxwell [11], which were provided by BNL for DCC17, were modified in order to add the Nb_3Sn coil. An iterative process, coupling magnetics and mechanics, has been used to optimize the conflicting objectives of increasing the coil mechanical stress while decreasing the transferred load to DCC17 and respecting the constraint of a 29 mm free aperture.

In consultation with BNL, the common coils are powered to produce a background field on the sample coil of 9.0 T. Fig. 4 shows the total magnetic B field distribution on both, DCC17 common coils and the testing coil.

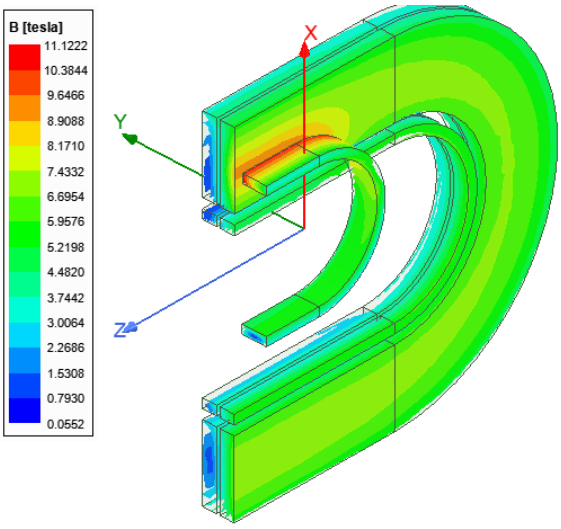

Fig. 4. Magnetic field distribution of DCC17 and the test coil distribution with I_{DCC17} = 10 kA

A. Mechanical Analysis

Fig. 2 shows the main components of the mechanical integration: the coil is placed in a casing (the "BigBOX"), which has two covers: a thin cover and a thick one. The case also has a non-magnetic central pole made of stainless steel 316L. The intended design was for the thin cover to remain load-free, while the thick cover was meant to bear the mechanical loads. The thick cover is 4 mm thick and made of 316 L stainless steel. It distributes the test-coil load across the DCC17 coil. The casing is attached to lateral bars. This mechanical connection uses PEEK bushings to electrically insulate the casing from the mechanical mounting. The casing is electrically floating with respect to the frame and the DCC17 magnet. The two lateral bars are attached to DCC17 end plates.

The mechanical properties considered for the static mechanical analysis, Young modulus, Poisson's ratio and integral thermal contraction, can be found in [12], except for those concerning the DCC17 magnet. The models and results for DCC17 are presented in [13]. In the absence of measurements for wax-impregnated coils, properties for epoxy-impregnated coils were used, homogenized isotropic material with a Young's modulus of 25 GPa.

Fig. 5 shows the DCC17 common coils normal stress, orthogonal to the cable flat surface on the top/left and parallel to the flat surface on the bottom/right. The mechanical load due to the test coil provokes an enhancement of 15 MPa on the stress

orthogonal to the flat surface and about 30 MPa on the stress parallel to the flat surface. These results were presented and discussed with BNL's staff.

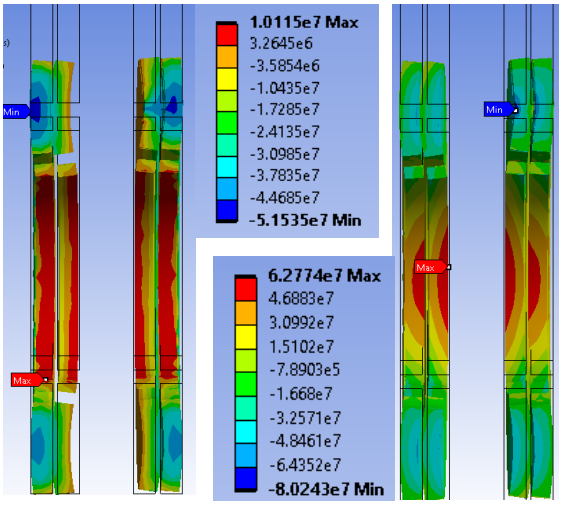

Fig. 5. DCC17 coil mechanical results. Top / left: Normal stress (edge of conductor). Bottom / right: Transversal stress (flat surface) in Pa.

Results from the 2D and 3D mechanical models show a good agreement with a difference, in terms of Von-Mises stress of about 5 MPa. Fig. 6 shows the Von-Mises stress on the test coil with 9.2 T background field resulting in a peak of 154 MPa.

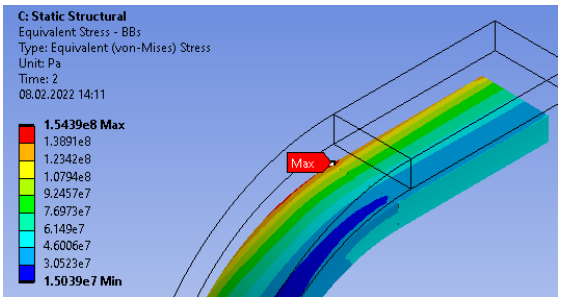

Fig. 6. High field region test coil Von-Mises stress.

Fig. 7 shows the worst-case scenario for the thick cover: 530 MPa of maximum principal stress. In case of inverted current, forces on the thin plate, the peak of maximum principal stress is 697 MPa.

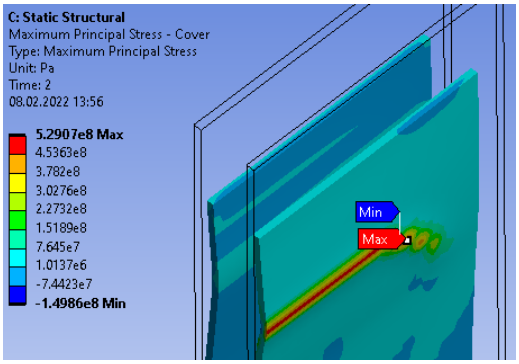

Fig. 7. High field region thick plate test coil maximum principal stress.

V. Manufacturing, Instrumentation and Electrical Tests

A. Coil manufacturing

As described previously, in order to benefit from the stress accumulation, the coil has been wound in its hard-way-bend direction. Before producing the final coil, a mockup version of 5 turns has been manufactured. Fig. 8 shows the winding of the final coil's last turn. Also lead and splice regions are shown.

Fig. 8. 13-turns coil winding process.

The case and covers were coated with Aremco SGC4000-HT, which is a commercial high temperature silicone-glass-ceramic based coating [14]. The coating requires a glazing step with a specific temperature protocol and maximum temperature of 720 °C. The glazing is done in air. The Rutherford cable is insulated with fiberglass.

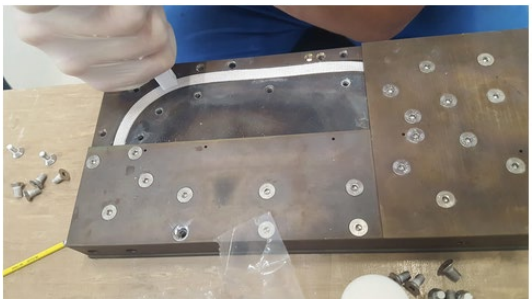

Fig. 9. Closing of the case - thin plate side.

Fig. 9 shows the closing of the case with the thin cover, which is split in three pieces, while the thick cover is made of only one piece. The reaction cycle is the one recommend by OST: HT of 210°C for 48 h + 400°C for 48 h + 665°C for 50 h. After reaction and instrumentation phase, the coil was impregnated in paraffin wax bath as described in [6]. Fig. 10 shows the coil being placed in an open-top container inside the vacuum vessel before impregnation. During the impregnation, the split cover was removed and a feeder layer inserted between coil and lid to feed the wax into the casing.

B. Instrumentation

To be able to identify quench locations, and thereby estimate the level of local mechanical stress and margin, each turn was

instrumented with a voltage tap, in additional to the v-taps on the leads. Fig. 11 presents a schematic view of voltage taps numbering. In addition to the voltage taps, acoustic sensors where mounted on the structure, as the one described in [15].

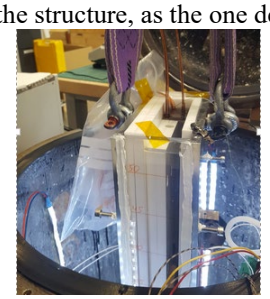

Fig. 10. Preparation for impregnation bath.

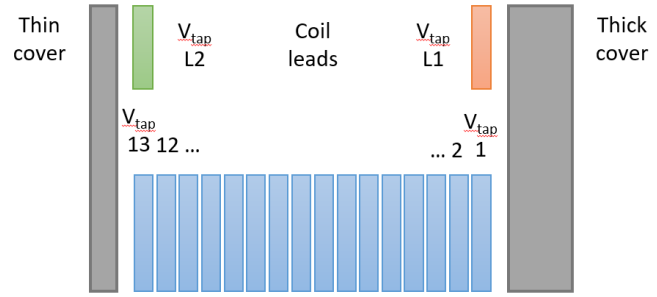

Fig. 11. Voltage taps numbering.

C. *Electrical test*

After the instrumentation and impregnation process a low resistance at room temperature was measured between the coil and its case. The coil was placed into our cryogen-free test station and cooled down to 4.2 K.

Fig. 12 shows the evolution of the coil to case resistance as a function of temperature. Varying from 60 kOhm to 300 – 500 kOhm at cold. The resistance was indirectly obtained by applying 1 µA and measuring the voltage to ground.

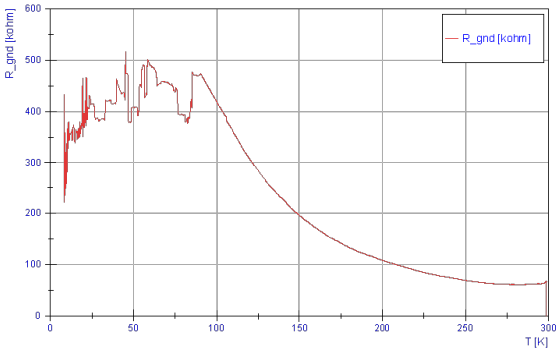

Fig. 12. Coil to case resistance as a function of temperature.

Additional tests were performed to ensure that the low resistance at room temperature came from one single location. It turns out that this spot is the lead number two. The problem could be caused by a fault in the insulation caused by the winding process and a fault in the insulation layer. The first issue could be solved by improving the winding method (less friction between insulation and structure), while the second could be solved by increasing the insulating layer thickness.

To mitigate any risk to the test facility, high pot tests were performed to ensure the insulation integrity between coil and its frame. With a maximum of 750 V, a resistance of 233 GOhm was measured.

VI. Extension for a Coil Current of Up to 20 kA

Thanks to a recent upgrade to the test facility, the coil could be tested with an electrical current up to 20 kA. We, therefore, decided to perform additional simulations to address the impact of this parameter on this study.

We choose five values of background field, from 7.0 to 9.0 T, resulting in different load lines of the test coil, and related coil stresses.

Fig. 13 shows the cable critical curves, with and without cabling degradation and coil load lines for different background fields.

By decreasing the background field, the coil short-sample increases. Consequently, the self-field also increases, resulting in a sizable change in total-field and mechanical stress distribution. By decreasing the background field, the coil maximum Von-Mises stress decreases, and the magnetic field margin increases, which is a much less interesting situation for testing the coil.

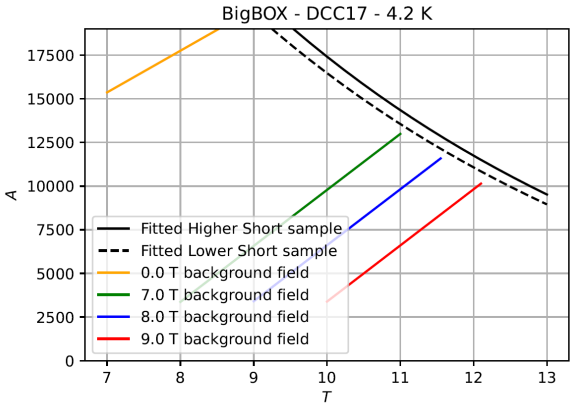

Fig. 13. Cable critical curves and coil load lines for different background fields and self-field.

VII. Test Results

During the BigBOX, and its integration into DCC17, test campaign, the demonstrator was powered 11 times. An overview of runs is showed in Fig. 14.

The colors are related to the background fields, and load lines, of Fig. 15: orange to represent the absence, green, blue and red to 7, 8 and 9 T background field.

As mentioned, Run #0 was performed without background field to the level of 13 kA. This run did not produce a BigBOX quench, and ended with the current ramp-down.

Run #1 was performed with a background field of 7 T and was performed by carrying out the following steps: First, DCC17 was ramped-up; once the field level of 7 T was achieved, BigBOX was powered until it quenched. The ramp rate used was 20 A/s. After the quench, the next run only started after the demonstrator and DCC17 magnets temperature were stabilized at 4.2 K.

Run #2, #3, #4 and #5 were performed in the same way and

following the same steps, except that the background field was different. Runs #2 and #5 were performed with 7 T, runs #3 and #4 with 8 T and run #3 with 9 T background field.

This sequence was choose because it allows, at first, to progressively increasing the demonstrator mechanical stress, due to the increase on the background field, to the maximum value of 160 MPa (9 T background field). Secondly, it allows regressively decreasing the demonstrator mechanical stress and verifying if a conductor permanent degradation occurred. As indicated in Fig. 14, and lately in Fig. 15, no permanent degradation was observed.

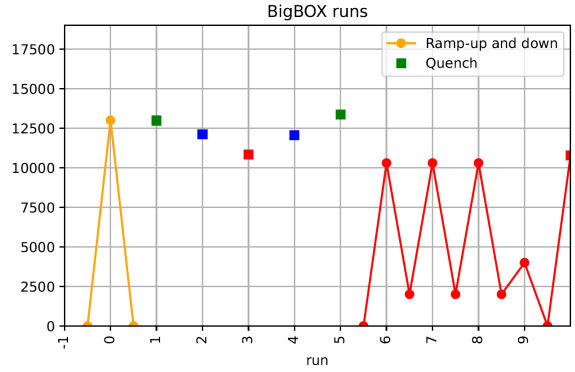

Fig. 14. BigBOX runs – colors are related to self-field or background fields of Fig. 13.

Next, we intended to increase and decrease BigBOX current, always keeping a constant background field of approximatively 9 T, with the goal of testing the demonstrator resilience to electromagnetic forces cycles. Therefore, Run #6, #7 and #8 were performed with a background field level of 9 T and maximum current of about 0.95*Irun#3. Run #9 ended before the current of 0.95*Irun#3 could be reached due to a power supply trip. Finally, with Run #10, we could ramp-up until it quenched, with the same background field of 9 T, to check if the quench current of Run #10 was the same as of Run #3.

Table 4 shows the measured DCC17 and BigBOX maximum currents for the 10 powering cycles. It should be noticed that the background field of Runs #1 and #5 are indicated as 7 T, but there is a variation of 2.2 % which leads to a variation of the same order of magnitude in the background field.

Similarly, as indicated in Table 4, Runs #2 and #4 have virtually the same electrical current, so we can conclude that on Run #4 BigBOX reached 99.5 % of its previous current.

Runs #3 and #10 were both presented with a background field of 9 T, but it is worth mentioning that on Run #10, DCC17 has 0.9 % less current. Even under less background field (about 0.1 T), BigBOX current is 0.7 % smaller on Run #10 with respect to Run #3.

TABLE 4
DCC17 AND BIGBOX MAXIMUM CURRENTS FOR THE 10 POWERING CYCLES

Run	I_{DCC17} in kA	I_{BigBOX} in kA
0	0.0	13.0
1*	7.195	12.979
2*	8.04	12.118
3*	9.124	10.845
4*	8.0393	12.06
5*	7.0398	13.359
6,7,8	9.0	10.3 – 2.0
10*	9.0395	10.769

* Runs ended due to quench of BigBOX.

Fig. 15 shows Runs #1-5 and #10, with the exact applied current, and computed magnetic field and the cable critical curve.

During the BigBOX manufacturing phase, no witness strand was reacted with the coil, so the demonstrator performance cannot be compared to its real critical curve. This is why, in Fig. 15, the two critical curves were obtained by fitting the measured points of reference [9]. The two curves represent the best and worst (higher and lower short sample) extracted strands.

Considering the reference of Fig. 11 and as mentioned in section IV.B , the stress-managed coil was designed such that, with background field, the forces from the testing coil would be transferred to DCC17 coils through the thick plate, so the local DCC17 coil strain remains small. In reality, however, before the BigBOX test campaign started, BigBOX current was accidentally inverted, so the forces were transferred through the thin plate. This is the reason why the mechanical stresses, on the demonstrator cross-section, of Fig. 17 slightly differs from the ones presented in section III.

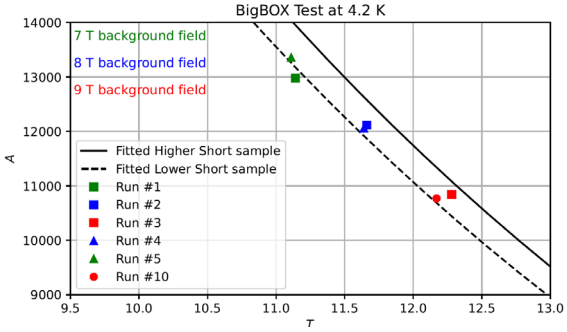

Fig. 15. BigBOX training runs and cable critical current – colors are related to background fields.

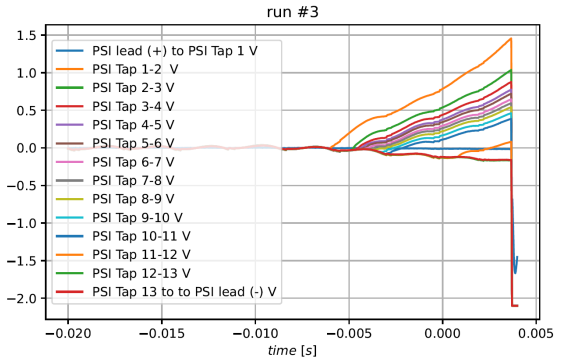

Fig. 16. Voltage taps evolution during quench detection for the Run #3.

So far, we carefully described the experiment in terms of reached electrical current and the computed demonstrator peak magnetic field but the quench locations were not presented.

All quenches happened on the first turn, voltage tap 1 in Fig. 11, which is, due to the inverted current, the high magnetic field

/ low stress region.

To illustrate the quench detection, Fig. 16 shows the Voltage taps evolution during quench detection for the Run #3.

VII. Discussion and Perspective

As highlighted on the previous section, even with a background field of 9 T (BigBOX peak field of 12.3 T), the demonstrator did not present strain related critical current reductions. As showed in Fig. 17, by increasing the background field (right), the total magnetic field on the high stress region (bottom) also increases. Therefore, the high stress turns have less load line margin when compared with the situation of 7 T background field.

It is important to notice that the peak of Von-Mises stress and magnetic field in Fig. 17 do not correspond to the ones presented in Fig. 4 and Fig. 6. This is due to the accidentally inversion on the current direction, which made the magnetic forces from BigBOX be transferred to DCC17 coils by means of the thin cover instead to the thick one, as we planned. Therefore, both cover and coil deformed more, which modified the level of mechanical stress. As for the magnetic field, the slightly non-symmetric mounting of BigBOX, with respect to DCC17, results in a small difference of its peak value.

As presented in Fig. 17, each turn of the demonstrator was submitted to a different stress and under distinct magnetic field. Another way of visualizing that is showed in Fig. 18 (top), where the peak of equivalent stress and peak of total magnetic field for the 13 turns during Run #3 is presented. Let us note that the Turn 1 presents a low level of stress and high magnetic field while Turn 13 presents a high level of stress and low magnetic field.

Fig. 18 (bottom) shows the linearized load line per turn during Run# 3, which shows the coil minimum performance in terms of engineering margin for a given computed Von-Mises stress. For instance, for a stress-level of 170 MPa, 29.5 % of engineering margin was enough in order to avoid quenching on turn 13, while for turn 10 (115 MPa), this number is 21.8 %.

An important BigBOX experiment perspective is its use to study Nb_3Sn permanent degradation over a large number of cycles. To do this, firstly, BigBOX is powered under background field until it quenches and its load line margin under background field is computed. Secondly, a large number of cycles is performed, which may provoke a permanent degradation on the high field / low stress turn.

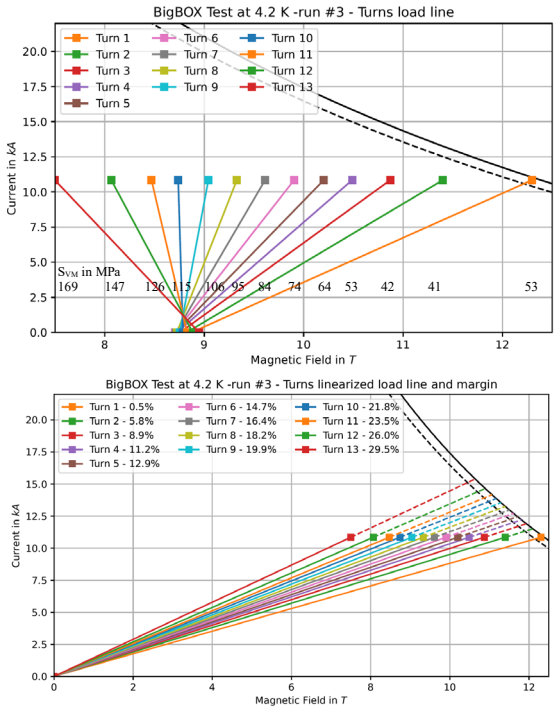

Fig. 18. Top: Peak of equivalent stress and peak of total magnetic field for the 13 turns during Run #3. Bottom: Linearized load line per turn during Run #3.

Finally, the demonstrator is powered again with its current inverted, so the high-field / low stress Turn of the previous experiment is now submitted to high magnetic field and its degradation measured. Through successive inversions of current and electromagnetic cycles, the degradation as a

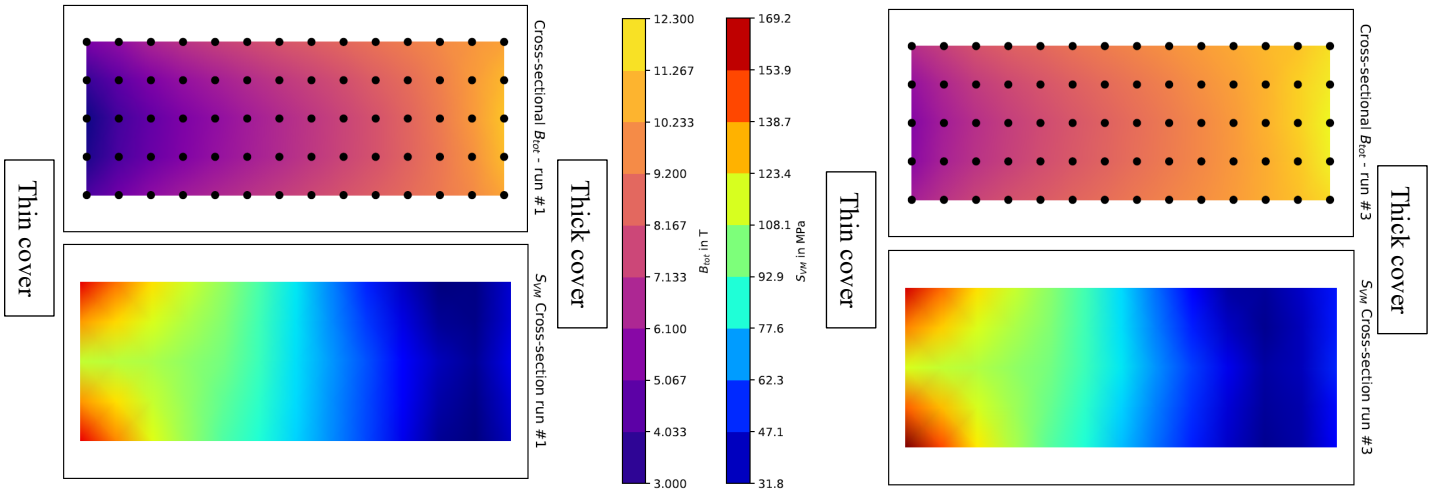

Fig. 17. Computed total magnetic field and Von-Mises stresses for runs #1 and #3.

function of the number of cycles can be measured.

V. Conclusions

We successfully design, manufactured and tested a racetrack stress-managed demonstrator mechanically and magnetic coupled to the BNL's dipole common coils DCC17. Systematically, the coil was powered to its estimated short sample, without any training behavior. The validation of manufacturing process, training performance, sliding interfaces, former ceramic coating insulation, among others, is an important step on the PSI LTS roadmap towards ultimate field stress-manages common coils. The roadmap includes subscale stress-managed common coil, and hybrid LTS/HTS tests.

VI. Acknowledgements

We would like to thank the Brookhaven National Laboratory for donating the cable and the Magnet Development Program of the US for funding the tests and contributing to the project. We also would like to thank the Lawrence Berkeley National Laboratory cabling team for providing the necessary information for the coil reaction. Our gratitude also goes to the PSI Magnet Section, in particular to M. Duda, for his contributions during cold measurements.

This work was performed under the auspices and with support from the Swiss Accelerator Research and Technology (CHART) program (www.chart.ch).

References

[1] The European Strategy Group, "Update of the European Strategy for Particle Physics." CERN-ESU-013, Jun. 2020.

[2] B. Auchmann *et al.*, "Electromechanical Design of a 16-T CCT Twin-Aperture Dipole for FCC," *IEEE Trans. Appl. Supercond.*, vol. 28, no. 3, pp. 1–5, Apr. 2018, doi: 10.1109/TASC.2017.2772898.

[3] A. McInturff *et al.*, "Current Status of the Texas A & M Magnet R & D Program," *IEEE Trans. Appl. Supercond.*, vol. 21, no. 3, pp. 1620–1623, Jun. 2011, doi: 10.1109/TASC.2010.2081654.

[4] N. Diaczenko *et al.*, "Stress management in high-field dipoles," in *Proceedings of the 1997 Particle Accelerator Conference (Cat. No.97CH36167)*, May 1997, pp. 3443–3445 vol.3. doi: 10.1109/PAC.1997.753236.

[5] A. Pampaloni *et al.*, "Preliminary Design of the Nb_3Sn $\cosþeta$ Short Model for the FCC," *IEEE Trans. Appl. Supercond.*, vol. 31, no. 5, pp. 1–5, Aug. 2021, doi: 10.1109/TASC.2021.3061334.

[6] M. Daly, "Improved Training in Paraffin-Wax Impregnated Nb_3Sn Rutherford Cables Demonstrated in BOX Samples," *Submitt. Publ. Supercond. Sci. Technol.*, 2020.

[7] R. Gupta *et al.*, "New Approach and Test Facility for High-Field Accelerator Magnets R&D," *IEEE Trans. Appl. Supercond.*, vol. 30, no. 4, pp. 1–6, Jun. 2020, doi: 10.1109/TASC.2019.2961064.

[8] S. A. Gourlay *et al.*, "Magnet R&D for the US LHC accelerator research program (LARP)," *IEEE Trans. Appl. Supercond.*, vol. 16, no. 2, pp. 324–327, 2006.

[9] E. Barzi *et al.*, "RRP Nb_3Sn strand studies for LARP," *Appl. Supercond. IEEE Trans. On*, vol. 17, pp. 2607–2610, Jul. 2007, doi: 10.1109/TASC.2007.899579.

[10] H. Felice *et al.*, "Development of MQYY: A 90-mm NbTi Double Aperture Quadrupole Magnet for HL-LHC," *IEEE Trans. Appl. Supercond.*, vol. 28, no. 3, pp. 1–5, Apr. 2018, doi: 10.1109/TASC.2018.2797941.

[11] "Ansys Maxwell | Electromechanical Device Analysis Software." https://www.ansys.com/products/electronics/ansys-maxwell (accessed Dec. 31, 2022).

[12] D. Martins Araujo *et al.*, "Magnetic and Mechanical 3-D Modelling of a 15 T Large Aperture Dipole Magnet," *IEEE Trans. Appl. Supercond.*, vol. 30, no. 4, pp. 1–5, Jun. 2020, doi: 10.1109/TASC.2020.2969639.

[13] R. Gupta *et al.*, "React and Wind Nb_3Sn Common Coil Dipole," *IEEE Trans. Appl. Supercond.*, vol. 17, no. 2, pp. 1130–1135, Jun. 2007, doi: 10.1109/TASC.2007.898139.

[14] "High Temperature Electrical Coatings & Sealants," p. 2, Aremco, Technical Bulletin A5-S1.

[15] M. Marchevsky, G. Sabbi, H. Bajas, and S. Gourlay, "Acoustic emission during quench training of superconducting accelerator magnets," *Cryogenics*, vol. 69, pp. 50–57, 2015.